Recombination line intensities for hydrogenic ions: The fine-structure components of H I and He II[*]

R.E.S. Clegg[1], S. Miller[2], P.J. Storey[2], and R. Kisielius[2]

[1] Particle Physics and Astronomy Research Council, Polaris House, North Star Avenue, Swindon, Wiltshire SN2 1SZ, UK
[2] Department of Physics and Astronomy, University College London, Gower Street, London WC1E 6BT, UK

Abstract. Emissivities have been calculated for fine-structure components of selected UV and optical recombination lines of H I and He II. Results are given for a range of electron temperatures and densities, and in Cases A and B of Baker & Menzel (1938). Relative intensities, wavelengths and velocity shifts of the fine-structure components are tabulated. Applications to the spectra of gaseous nebulae are discussed. Depending on the temperature, density and Case, the centres of unresolved lines can shift by up to $0.9 \, \mathrm{km \, s^{-1}}$ for H I and $3.3 \, \mathrm{km \, s^{-1}}$ for He II. A new calibration of the Hα–[N II] method for determining electron temperatures is given.

Key words: atomic data — line: formation — line: profiles — H II regions — planetary nebulae: general

1. Introduction

Recombination lines of hydrogen and helium in the optical, IR and UV spectral regions are frequently used in astronomical spectroscopy for measurements of radial velocities and velocity fields. The levels of hydrogenic ions are not quite degenerate, and lines such as Hα ($n = 3 \to 2$) and He II 4686 Å ($n = 4 \to 3$) consists of many components; for example for Hα there are seven components, with transitions between the $3\mathrm{d} \, ^2\mathrm{D}_{5/2,3/2}$, $3\mathrm{p} \, ^2\mathrm{P}_{3/2,1/2}$ and $3\mathrm{s} \, ^2\mathrm{S}_{1/2}$ in $n = 3$ and $2\mathrm{p} \, ^2\mathrm{P}_{3/2,1/2}$ and $2\mathrm{s} \, ^2\mathrm{S}_{1/2}$ in $n = 2$, subject to the usual selection rules for dipole allowed transitions. He II $\lambda4686$ Å has thirteen components.

The precise energies of these levels in hydrogenic ions depend on relativistic shifts as well as fine-structure effects derived from the spin-orbit interaction and quantum electrodynamic effects such as the Lamb shift. For example, the $2\mathrm{s} \, ^2\mathrm{S}_{1/2}$ and $2\mathrm{p} \, ^2\mathrm{P}_{1/2}$ states of H I are separated by $0.0353 \, \mathrm{cm^{-1}}$ due to QED effects, while the $2\mathrm{p} \, ^2\mathrm{P}_{1/2}$ and $2\mathrm{p} \, ^2\mathrm{P}_{3/2}$ states are separated by $0.3659 \, \mathrm{cm^{-1}}$ due to the spin-orbit interaction.

Unless the line components are resolved, their effect is to broaden the spectral lines and to produce small shifts in the effective position of the line centre, depending on the distribution of intensities between the components. As we show below, the range covered by the line components is $9.1 \, \mathrm{km \, s^{-1}}$ for hydrogen and $36.6 \, \mathrm{km \, s^{-1}}$ for helium lines. In an atom of mass m at temperature T_e, the full line width ($FWHM$) of a single component in velocity units due to thermal broadening is $(8kT_\mathrm{e} \ln 2/m)^{1/2}$. For H I and He II, this width has the values of 21.4 and $10.7 \, \mathrm{km \, s^{-1}}$ at $10^4 \, \mathrm{K}$, and 6.8 and $3.4 \, \mathrm{km \, s^{-1}}$ at $10^3 \, \mathrm{K}$, respectively. Hence the fine-structure broadening can affect line widths of hydrogen and especially helium recombination lines in cool ($T_\mathrm{e} \sim 10^3 \, \mathrm{K}$) plasmas. Although many planetary nebulae are somewhat warmer, with $T_\mathrm{e} \sim 10^4 \, \mathrm{K}$, H II regions often have $T_\mathrm{e} \sim 5000 \, \mathrm{K}$ and some old novae have electron temperatures as low as $500 \, \mathrm{K}$ (e.g., DQ Her, Williams et al. 1978).

Because of the combined effects of thermal, turbulent and expansion broadening, we do not expect these components to be completely resolved in observations of ionized plasmas in space. However, they are resolved in laboratory experiments using laser techniques (e.g., Hänsch et al. 1975).

We give several examples of the significance of these splittings. Dyson & Meaburn (1971) showed that the fine-structure of the Hα line profile makes a significant difference to derived electron temperatures in nebulae when these are obtained from the ratio of observed widths of the [N II]6584 Å and Hα lines. In a typical example, the temperature derived for the Orion region changed from 6200 to 7350 K, which would alter the derived O/H ratio

(from [O II]3727 Å) by a factor 2.6. In the present paper we update the Hα – [N II] correction scheme.

A second application is provided by supernova 1987A. Cumming & Meikle (1993) detected a remarkable short-lived narrow component in Hα and Hβ emission from the circumstellar medium of the supernova. In some spatial positions the narrow component's $FWHM$ was as low as 5.3 ± 1.3 km s^{-1}, which after allowance for the Hα fine-structure suggests emission from extremely cool recombining gas. In fact, the formal best fit at some positions was narrower than the spread of the fine-structure components. Of several models discussed, one involved illumination of a circumstellar H I cloud by the H Lyβ emission line (absorption of Lyβ would only populate the 3p level, and thus the number of components making up the Hα line would be reduced).

Other studies have revealed narrow emission lines from ionized regions. Onello & Phillips (1993) observed emission components with $FWHM$ as low as 3.6 km s^{-1} in the H 168α recombination line towards galactic sources; such components if seen in the Balmer lines would be affected by the fine-structure we discuss here. Gallagher & Hunter (1983) studied widths of the Hα line in extragalactic H II regions. Observed widths were corrected for instrumental and thermal broadening, and the "excess widths" due to the bulk gas velocity dispersion were as small as $1.6 - 13.0$ km s^{-1} ($FWHM$) for some positions in NGC 4214. Correction for fine-structure broadening would reduce these excesses still further.

Lastly, we show below that the He II line at 1640 Å has seven components spanning a range of 36.6 km s^{-1} (with the two strongest components 26 km s^{-1} apart). Laming & Feldman (1993) analysed $SKYLAB$ spectra of a Solar Prominence which partially resolved the 7 components, and were able to derive information on the process populating the He II $n = 3$ levels in the hot plasma.

Calculations of the recombination spectra of hydrogenic ions in Case B of Baker & Menzel (1938) have been described by Hummer & Storey (1987), Storey & Hummer (1988) and Storey & Hummer (1995) (hereafter HS, SH and SH95). Their calculations take full account of all radiative and collisional processes, and they tabulated emissivities at a range of electron temperatures and densities for principal quantum numbers up to $n = 50$.

Martin (1988) presented effective recombination coefficients for H I and He II states as a function of n and ℓ, from which the relative intensities of fine-structure components can be derived, but only for the "zero density" case, in which all collisional processes are ignored. Effective recombination coefficients for hydrogen have also been calculated by Smits (1991) as a function of both electron temperature and density. His calculations extend the calculations of Hummer & Storey (1987) to low electron temperatures, $312.5\,\mathrm{K} \leq T_e \leq 2500\,\mathrm{K}$, using essentially the same methods. He does not, however, treat He II, or

give the ℓ-dependent information necessary to calculate the intensities of the fine-structure components.

In this paper we summarize the effects of the fine-structure components and present new calculations of their relative intensities, as a function of electron temperature and density, and in Cases A and B. We also include synthetic spectra showing the components in velocity space, and tabulate the shifts of the line centres for different densities, temperatures and Cases.

2. Adopted energy levels and "reference" wavelengths

For H I and He II energy levels we adopt the values given by Erickson (1977). These are based on quantum electrodynamic calculations including the Lamb shift. This work makes a careful comparison between experimental and calculated energy-level differences, and demonstrates good agreement. In general the theoretical QED uncertainty is smaller than the experimental error.

For each transition of H I and He II considered, we adopted a *reference wavelength*, λ_{ref}, for use as a zero-point in the presentation of the shifts of individual component lines in velocity space. These were computed from the Rydberg formula

$$\lambda_{\mathrm{ref}} = \left[\mu R_\infty \left(n_l^{-2} - n_u^{-2} \right) \right]^{-1}, \qquad (1)$$

where $R_\infty = 109737.3153$ cm^{-1} is the Rydberg constant for infinite nuclear mass (Ferguson 1986), and μ is the reduced mass of the electron-nucleus system in electron masses. The finite mass Rydberg constants, μR_∞, that were used to calculate the reference wavelengths are 109677.6155, 109707.4343, 109717.3590 and 109722.2772 cm^{-1} for ^{1}H, ^{2}D, ^{3}He and ^{4}He respectively.

The difference in energy, Δ_{nj}, between the energy of a hydrogenic state E_n, given by the Rydberg formula and the energy E_{nj} obtained from the Dirac equation is approximately

$$\Delta_{nj} = E_{nj} - E_n = -\frac{Z^4 \alpha^4}{n^4} \; \mu R_\infty \left(\frac{n}{j + \frac{1}{2}} - \frac{3}{4} \right), \qquad (2)$$

where α is the fine-structure constant and terms in higher powers of $(Z\alpha)$ have been neglected. This equation describes the relativistic energy shifts of the hydrogenic levels (the mass correction and the Darwin term) as well as the fine-structure due to the spin-orbit interaction. The Lamb shift is not included but can be neglected for the argument made here. For a given n, $(j + \frac{1}{2})$ runs from one to n, so that the bracket in Eq. (2) is always positive. Thus the levels $n\ell j$ always lie energetically lower than the corresponding non-relativistic energies given from the Rydberg formula. In addition, the energy shift Δ_{nj} falls rapidly as n increases. As a consequence, the fine-structure components in any transition $n_u \to n_l$ will generally be displaced to wavelengths shorter than λ_0 as given by Eq. (1), and the corresponding velocity shifts will usually be negative.

We ignore hyperfine structure in this work. Its effect is to double the energy levels of ^{1}H and ^{3}He, which have finite nuclear spin. The typical splitting is only 0.001 cm^{-1}, which corresponds to a velocity splitting of 0.02 km s^{-1} for optical and UV lines, and is thus neglected.

Table 1 lists, for some commonly observed transitions of H and He, the number of components N_c, the total range in velocity space of the components Δv, and the reference wavelength, defined as above, for the four isotopes ^{1}H, ^{2}D, ^{3}He and ^{4}He. We stress that the reference wavelength does not represent any mean wavelength for the line in question, but is simply a reference point to anchor our chosen scale of velocity shifts. Here, and throughout this paper, wavelengths are given in air for $\lambda > 2000$ Å and in vacuum otherwise. The variation of the velocity range of the components as a function of nuclear mass (e.g. between ^{1}H and ^{2}H, or ^{3}He and ^{4}He) is too small to be recorded in Table 1.

3. Calculation of level populations and emissivities

3.1. Calculation of $b_{n\ell}$

As in earlier calculations (HS and SH), we work in terms of the departure coefficients, $b_{n\ell}$, defined in terms of the Saha-Boltzmann populations at electron temperature T_e by

$$\frac{N_{n\ell}}{N_e N_+} = \frac{\omega_{n\ell}}{2\omega_+} \left(\frac{h^2}{2\pi mkT_e}\right)^{3/2} e^{x_{n\ell}} b_{n\ell}, \qquad (3)$$

where N_e and N_+ are the number densities of electrons and recombining ions respectively, $x_{n\ell} = E_{n\ell}/kT_e$, and $E_{n\ell}$ is the ionization energy of the state with quantum numbers n, ℓ. The statistical weights of this state and of the ion ground state are $\omega_{n\ell}$ and ω_+. A two stage process is used to compute the values of $b_{n\ell}$.

In the first stage, it is assumed that for a given n the states $n\ell$ are populated in proportion to their statistical weight, so that $b_{n\ell} = b_n$ for all ℓ. This calculation is complete in the sense that a matrix condensation method is used to reduce the infinite set of algebraic equations determining the b_n to a finite set. All spontaneous radiative processes and electron induced collisional processes are included. The approximations used for these rates were given in HS.

In the second stage, the equations that determine $b_{n\ell}$ are solved by an iterative procedure. Above some limiting principal quantum number ($n = n_c$), we assume that $b_{n\ell} = b_n$ and the values calculated in the first stage are used. For $n \leq n_c$, the values of $b_{n\ell}$ are determined explicitly including the effects of ℓ-changing collisions. The effect of collisions with electrons, protons and ionized helium atoms are included. For the calculation of the hydrogen spectrum, we assume that helium is singly ionized, whereas for the He II spectrum, we assume helium is doubly ionized. The helium abundance is taken to be 10% of

that of hydrogen. An iterative solution for the $b_{n\ell}$ is carried out, starting at $n = n_c$ and ending at $n = 2$ with a maximum of twenty iterations being carried out. Above $n = 50$, the values of $b_{n\ell}$ are interpolated as a function of n. This interpolation scheme and the approximations used for the required ℓ-dependent rate coefficients are described in HS.

3.2. Calculation of emissivities for fine-structure components

The calculation of $b_{n\ell}$ described in Sect. 2.1 allows us to determine the emissivity in the hydrogenic transition $n_u\ell_u \to n_l\ell_l$;

$$\varepsilon(n_u\ell_u \to n_l\ell_l) = N(n_u\ell_u)A(n_u\ell_u \to n_l\ell_l)h\nu_{ul}, \qquad (4)$$

where A is a radiative transition probability and $h\nu_{ul}$ is the transition energy. The emissivity of a fine-structure component of this transition is

$$\begin{aligned}\varepsilon(n_u\ell_u j_u \to n_l\ell_l j_l) = \; & N(n_u\ell_u j_u) \times \\ & \times A(n_u\ell_u j_u \to n_l\ell_l j_l) h\nu_{ul}.\end{aligned} \qquad (5)$$

In LS-coupling, the transition probabilities in Eqs. (4) and (5) are related by

$$\begin{aligned}A(n_u\ell_u j_u \to n_l\ell_l j_l) = \; & (2j_l+1)(2\ell_u+1) \times \\ & \times \begin{Bmatrix} j_u & j_l & 1 \\ \ell_l & \ell_u & \frac{1}{2} \end{Bmatrix}^2 A(n_u\ell_u \to n_l\ell_l),\end{aligned} \qquad (6)$$

where { } is a 6-j symbol as defined for example by Brink & Satchler (1968). In this expression we have assumed that the fine-structure energy shifts are negligible compared to the transition energies. We further assume that $b_{n\ell j} = b_{n\ell}$, with the values of $b_{n\ell}$ being calculated as described above. This is equivalent to the assumption that the j-levels associated with a particular $n\ell$ are populated according to their statistical weights $(2j+1)$.

Techniques for the rapid calculation of the values of $A(n_u\ell_u \to n_l\ell_l)$ have been described by Storey & Hummer (1991).

4. Results

We have computed recombination coefficients in Case A and Case B for Hα ($n = 3 \to 2$), Hβ ($n = 4 \to 2$), Hγ ($n = 5 \to 2$); and He II 4686 Å ($n = 4 \to 3$), 3203 Å ($n = 5 \to 3$), 1640 Å ($n = 3 \to 2$) and 1215 Å ($n = 4 \to 2$). These were selected either as strong optical lines that are commonly used for velocity measurements, or as strong ultraviolet lines which can be resolved by the Hubble Space Telescope. For hydrogen, the selected ranges of electron density and temperature are $10^2 - 10^9$ cm^{-3} and $300 - 30\,000$ K. For He II these ranges are $10^4 - 10^9$ cm^{-3}, and $1000 - 30\,000$ K. The temperature range spans that seen in photo-ionized nebulae, from novae (T_e down to 300 K) to the hottest planetary nebulae ($T_e \sim 25\,000$ K).

Table 1. Summary of components, and reference wavelengths of hydrogenic transitions

			Δv (km s^{-1})		Reference wavelengths λ_{ref} (Å)			
n_{u}	n_{l}	N_{c}	H I	He II	^{1}H I	^{2}H I	^{3}He II	^{4}He II
2	1	2	1.33	5.33	1215.6841	1215.3537	303.8109	303.7973
3	1	2	0.33	1.33	1025.7335	1025.4547	256.3405	256.3290
4	1	2	0.13	0.53	972.5473	972.2829	243.0487	243.0379
5	1	2	0.07	0.27	949.7532	949.4951	237.3523	237.3417
6	1	2	0.04	0.15	937.8134	937.5585	234.3684	234.3579
3	2	7	9.12	36.64	6562.8812	6561.0974	1640.5790	1640.5055
4	2	7	5.93	23.78	4861.3784	4860.0571	1215.2437	1215.1893
5	2	7	5.04	20.17	4340.5086	4339.3288	1085.0391	1084.9904
6	2	7	4.65	18.61	4101.7762	4100.6613	1025.3619	1025.3159
4	3	13	8.65	34.62	18751.1492	18746.0526	4686.0572	4685.8471
5	3	13	5.54	22.19	12818.1620	12814.6780	3203.3302	3203.1867
6	3	13	4.73	18.94	10938.1610	10935.1880	2733.4893	2733.3668
5	4	19	8.39	33.55	40511.7561	40500.7449	10124.2560	10123.8022
6	4	19	5.04	20.15	26251.6145	26244.4793	6560.5039	6560.2098
6	5	25	8.27	33.02	74578.4650	74558.1943	18637.8548	18637.0193

Table 2a. Fine structure components for $n \to 2$ transitions

Index	Transition			ℓ_{u}	$2j_{\text{u}}$	ℓ_{l}	$2j_{\text{l}}$
1	ns ^{2}S$_{1/2}$	–	2p ^{2}P$^{\text{o}}_{1/2}$	0	1	1	1
2	ns ^{2}S$_{1/2}$	–	2p ^{2}P$^{\text{o}}_{3/2}$	0	1	1	3
3	np ^{2}P$^{\text{o}}_{1/2}$	–	2s ^{2}S$_{1/2}$	1	1	0	1
4	np ^{2}P$^{\text{o}}_{3/2}$	–	2s ^{2}S$_{1/2}$	1	3	0	1
5	nd ^{2}D$_{3/2}$	–	2p ^{2}P$^{\text{o}}_{1/2}$	2	3	1	1
6	nd ^{2}D$_{3/2}$	–	2p ^{2}P$^{\text{o}}_{3/2}$	2	3	1	3
7	nd ^{2}D$_{5/2}$	–	2p ^{2}P$^{\text{o}}_{3/2}$	2	5	1	3

Table 2b. Fine structure components for $n \to 3$ transitions

Index	Transition			ℓ_{u}	$2j_{\text{u}}$	ℓ_{l}	$2j_{\text{l}}$
1	ns ^{2}S$_{1/2}$	–	3p ^{2}P$^{\text{o}}_{1/2}$	0	1	1	1
2	ns ^{2}S$_{1/2}$	–	3p ^{2}P$^{\text{o}}_{3/2}$	0	1	1	3
3	np ^{2}P$^{\text{o}}_{1/2}$	–	3s ^{2}S$_{1/2}$	1	1	0	1
4	np ^{2}P$^{\text{o}}_{3/2}$	–	3s ^{2}S$_{1/2}$	1	3	0	1
5	np ^{2}P$^{\text{o}}_{1/2}$	–	3d ^{2}D$_{3/2}$	1	1	2	3
6	np ^{2}P$^{\text{o}}_{3/2}$	–	3d ^{2}D$_{3/2}$	1	3	2	3
7	np ^{2}P$^{\text{o}}_{3/2}$	–	3d ^{2}D$_{5/2}$	1	3	2	5
8	nd ^{2}D$_{3/2}$	–	3p ^{2}P$^{\text{o}}_{1/2}$	2	3	1	1
9	nd ^{2}D$_{3/2}$	–	3p ^{2}P$^{\text{o}}_{3/2}$	2	3	1	3
10	nd ^{2}D$_{5/2}$	–	3p ^{2}P$^{\text{o}}_{3/2}$	2	5	1	3
11	nf ^{2}F$^{\text{o}}_{5/2}$	–	3d ^{2}D$_{3/2}$	3	5	2	3
12	nf ^{2}F$^{\text{o}}_{5/2}$	–	3d ^{2}D$_{5/2}$	3	5	2	5
13	nf ^{2}F$^{\text{o}}_{7/2}$	–	3d ^{2}D$_{5/2}$	3	7	2	5

The density values range from a typical H II region value of $100\,\text{cm}^{-3}$ to a value typical of the ionized gas around symbiotic stars.

In Table 2 we define an index for each line component. For transitions from $n \to 2$ there are seven components, and for $n \to 3$ there are thirteen. The states involved in the transition are described by their values of ℓ and j.

The indices defined in Tables 2a and 2b are used to identify the line components in our principal set of results. These are listed in Tables 3a–g for Baker & Menzel's Case B, and in Tables 4a–g for Case A. The full tables are only available in electronic form. Here we present only Tables 3a and 4a. For each line, the reference wavelength (defined in Sect. 2) defines zero velocity for the line components. The shift in wavelength ($\Delta\lambda$) and in velocity (Δv) is listed for each component. Normalized intensities (which sum to unity over the vertical columns of Tables 3 and 4) are listed for the adopted ranges of electron temperature and density for H I and He II.

It must be emphasized that the reference wavelength does not represent any mean wavelength for the line in question, but is simply a reference point to anchor our chosen scale of velocity shifts. Most of the shifts are negative for the reasons given in Sect. 2.

Tables 5a–d show our computed emissivities for $n_{\text{u}} \to n_{\text{l}}$ transitions, in units of erg cm^3 s^{-1}, for the full range of electron densities and temperatures considered. From these, the absolute emissivity of any component listed in Tables 3 and 4 can be computed: the normalized intensities listed there should be multiplied by the total emissivity from Table 5.

Table 3. Normalized component intensities for Hα: H $3 \to 2$; $\lambda_{\text{ref}} = 6562.8812$ Å; Case B

N_e [cm^{-3}]	Index	$\Delta\lambda$ [Å]	Δv [km s^{-1}]	T[K] 300	1000	3000	10 000	30 000
10^2	1	$-.130$	-5.93	.018	.023	.031	.044	.061
	2	.028	1.27	.036	.046	.061	.088	.121
	3	$-.110$	-5.03	.057	.069	.085	.106	.125
	4	$-.157$	-7.16	.113	.138	.170	.213	.250
	5	$-.172$	-7.85	.259	.241	.218	.183	.148
	6	$-.014$	-0.65	.052	.048	.044	.037	.030
	7	$-.030$	-1.36	.465	.435	.392	.330	.266
10^4	1	$-.130$	-5.93	.021	.025	.032	.044	.061
	2	.028	1.27	.042	.049	.063	.088	.121
	3	$-.110$	-5.03	.064	.073	.087	.107	.125
	4	$-.157$	-7.16	.129	.147	.175	.215	.250
	5	$-.172$	-7.85	.248	.235	.214	.182	.147
	6	$-.014$	-0.65	.050	.047	.043	.036	.029
	7	$-.030$	-1.36	.447	.423	.386	.328	.265
10^6	1	$-.130$	-5.93	.026	.028	.034	.045	.060
	2	.028	1.27	.052	.057	.067	.089	.121
	3	$-.110$	-5.03	.079	.084	.094	.110	.126
	4	$-.157$	-7.16	.159	.168	.187	.220	.252
	5	$-.172$	-7.85	.228	.221	.206	.179	.147
	6	$-.014$	-0.65	.046	.044	.041	.036	.029
	7	$-.030$	-1.36	.410	.398	.371	.322	.265
10^7	1	$-.130$	-5.93	.029	.031	.035	.045	.060
	2	.028	1.27	.058	.061	.070	.089	.119
	3	$-.110$	-5.03	.090	.092	.099	.113	.127
	4	$-.157$	-7.16	.181	.185	.198	.225	.253
	5	$-.172$	-7.85	.214	.210	.199	.176	.147
	6	$-.014$	-0.65	.043	.042	.040	.035	.029
	7	$-.030$	-1.36	.385	.379	.359	.317	.265
10^8	1	$-.130$	-5.93	.025	.027	.032	.041	.055
	2	.028	1.27	.050	.055	.063	.081	.110
	3	$-.110$	-5.03	.106	.105	.109	.118	.130
	4	$-.157$	-7.16	.211	.210	.217	.237	.260
	5	$-.172$	-7.85	.203	.201	.193	.174	.149
	6	$-.014$	-0.65	.041	.040	.039	.035	.030
	7	$-.030$	-1.36	.365	.361	.347	.314	.268
10^9	1	$-.130$	-5.93	.014	.016	.019	.025	.035
	2	.028	1.27	.028	.032	.037	.049	.070
	3	$-.110$	-5.03	.103	.107	.113	.124	.137
	4	$-.157$	-7.16	.206	.213	.226	.248	.275
	5	$-.172$	-7.85	.216	.211	.202	.185	.161
	6	$-.014$	-0.65	.043	.042	.040	.037	.032
	7	$-.030$	-1.36	.390	.379	.363	.332	.290

Table 4. Normalized component intensities for Hα: H $3 \rightarrow 2$; $\lambda_{\mathrm{ref}} = 6562.8812$ Å; Case A

N_{e} [cm^{-3}]	Index	$\Delta\lambda$ [Å]	Δv [km s^{-1}]	T[K] 300	1000	3000	10 000	30 000
10^2	1	$-.130$	-5.93	.012	.016	.024	.040	.066
	2	.028	1.27	.024	.032	.048	.080	.132
	3	$-.110$	-5.03	.008	.010	.013	.018	.024
	4	$-.157$	-7.16	.016	.020	.027	.037	.048
	5	$-.172$	-7.85	.314	.307	.296	.275	.243
	6	$-.014$	-0.65	.063	.061	.059	.055	.049
	7	$-.030$	-1.36	.564	.553	.533	.495	.438
10^4	1	$-.130$	-5.93	.014	.018	.025	.041	.067
	2	.028	1.27	.028	.036	.050	.082	.134
	3	$-.110$	-5.03	.009	.011	.014	.019	.024
	4	$-.157$	-7.16	.019	.022	.028	.038	.048
	5	$-.172$	-7.85	.310	.305	.294	.274	.242
	6	$-.014$	-0.65	.062	.061	.059	.055	.048
	7	$-.030$	-1.36	.558	.548	.530	.493	.436
10^6	1	$-.130$	-5.93	.020	.022	.029	.043	.069
	2	.028	1.27	.040	.045	.057	.087	.137
	3	$-.110$	-5.03	.012	.013	.015	.020	.024
	4	$-.157$	-7.16	.024	.026	.031	.039	.049
	5	$-.172$	-7.85	.301	.298	.289	.270	.240
	6	$-.014$	-0.65	.060	.060	.058	.054	.048
	7	$-.030$	-1.36	.543	.536	.521	.487	.433
10^7	1	$-.130$	-5.93	.024	.026	.032	.046	.070
	2	.028	1.27	.048	.052	.063	.091	.140
	3	$-.110$	-5.03	.014	.015	.017	.020	.025
	4	$-.157$	-7.16	.029	.030	.033	.040	.049
	5	$-.172$	-7.85	.295	.292	.285	.267	.239
	6	$-.014$	-0.65	.059	.058	.057	.053	.048
	7	$-.030$	-1.36	.531	.526	.513	.481	.430
10^8	1	$-.130$	-5.93	.023	.026	.032	.045	.069
	2	.028	1.27	.046	.052	.063	.090	.137
	3	$-.110$	-5.03	.018	.018	.019	.022	.025
	4	$-.157$	-7.16	.037	.036	.038	.044	.051
	5	$-.172$	-7.85	.292	.289	.283	.266	.239
	6	$-.014$	-0.65	.058	.058	.057	.053	.048
	7	$-.030$	-1.36	.526	.520	.509	.479	.431
10^9	1	$-.130$	-5.93	.011	.014	.018	.028	.047
	2	.028	1.27	.023	.027	.036	.056	.094
	3	$-.110$	-5.03	.027	.026	.026	.028	.032
	4	$-.157$	-7.16	.054	.052	.052	.056	.063
	5	$-.172$	-7.85	.295	.294	.289	.277	.255
	6	$-.014$	-0.65	.059	.059	.058	.055	.051
	7	$-.030$	-1.36	.531	.529	.521	.499	.458

Table 5a. H I line emissivities [erg cm^3 s^{-1}]: Case B

$n_u - n_l$	N_e [cm^{-3}]	300	1000	3000	10 000	30 000
3 − 2	10^2	6.796(−24)	2.617(−24)	1.048(−24)	3.537(−25)	1.199(−25)
	10^4	7.440(−24)	2.655(−24)	1.047(−24)	3.530(−25)	1.199(−25)
	10^6	1.026(−23)	2.859(−24)	1.057(−24)	3.522(−25)	1.198(−25)
	10^7	1.472(−23)	3.174(−24)	1.081(−24)	3.526(−25)	1.197(−25)
	10^8	2.660(−23)	3.894(−24)	1.144(−24)	3.557(−25)	1.198(−25)
	10^9	6.754(−23)	5.703(−24)	1.309(−24)	3.685(−25)	1.211(−25)
4 − 2	10^2	1.613(−24)	7.146(−25)	3.265(−25)	1.235(−25)	4.440(−26)
	10^4	1.959(−24)	7.623(−25)	3.331(−25)	1.240(−25)	4.443(−26)
	10^6	3.125(−24)	8.974(−25)	3.512(−25)	1.255(−25)	4.450(−26)
	10^7	4.849(−24)	1.055(−24)	3.712(−25)	1.272(−25)	4.459(−26)
	10^8	9.658(−24)	1.401(−24)	4.143(−25)	1.317(−25)	4.514(−26)
	10^9	2.666(−23)	2.227(−24)	5.049(−25)	1.409(−25)	4.625(−26)
5 − 2	10^2	6.677(−25)	3.078(−25)	1.469(−25)	5.784(−26)	2.123(−26)
	10^4	8.296(−25)	3.323(−25)	1.506(−25)	5.818(−26)	2.124(−26)
	10^6	1.394(−24)	4.042(−25)	1.614(−25)	5.917(−26)	2.128(−26)
	10^7	2.300(−24)	4.969(−25)	1.753(−25)	6.072(−26)	2.144(−26)
	10^8	5.056(−24)	7.188(−25)	2.079(−25)	6.487(−26)	2.206(−26)
	10^9	1.488(−23)	1.223(−24)	2.674(−25)	7.038(−26)	2.205(−26)

Table 5b. He II line emissivities [erg cm^3 s^{-1}]: Case B

$n_u - n_l$	N_e [cm^{-3}]	1000	3000	10 000	30 000
3 − 2	10^4	6.263(−23)	2.630(−23)	9.790(−24)	3.701(−24)
	10^6	7.097(−23)	2.701(−23)	9.790(−24)	3.692(−24)
	10^7	8.268(−23)	2.811(−23)	9.832(−24)	3.687(−24)
	10^8	1.086(−22)	3.049(−23)	9.962(−24)	3.687(−24)
	10^9	1.733(−22)	3.575(−23)	1.030(−23)	3.702(−24)
4 − 2	10^4	1.459(−23)	6.939(−24)	2.991(−24)	1.264(−24)
	10^6	1.842(−23)	7.557(−24)	3.063(−24)	1.271(−24)
	10^7	2.308(−23)	8.231(−24)	3.140(−24)	1.280(−24)
	10^8	3.277(−23)	9.431(−24)	3.270(−24)	1.293(−24)
	10^9	5.657(−23)	1.176(−23)	3.504(−24)	1.319(−24)
4 − 3	10^4	1.263(−23)	4.766(−24)	1.492(−24)	4.623(−25)
	10^6	1.309(−23)	4.612(−24)	1.444(−24)	4.536(−25)
	10^7	1.418(−23)	4.554(−24)	1.406(−24)	4.459(−25)
	10^8	1.699(−23)	4.600(−24)	1.362(−24)	4.356(−25)
	10^9	2.434(−23)	4.935(−24)	1.327(−24)	4.232(−25)
5 − 3	10^4	3.825(−24)	1.662(−24)	6.149(−25)	2.169(−25)
	10^6	4.551(−24)	1.741(−24)	6.166(−25)	2.161(−25)
	10^7	5.381(−24)	1.820(−24)	6.177(−25)	2.152(−25)
	10^8	7.066(−24)	1.965(−24)	6.205(−25)	2.136(−25)
	10^9	1.114(−23)	2.271(−24)	6.315(−25)	2.117(−25)

Table 5c. H I line emissivities [erg cm^3 s^{-1}]: Case A

	N_e	T[K]				
$n_u - n_l$	[cm^{-3}]	300	1000	3000	10 000	30 000
$3 - 2$	10^2	5.494(−24)	2.031(−24)	7.615(−25)	2.327(−25)	7.160(−26)
	10^4	5.670(−24)	1.988(−24)	7.449(−25)	2.297(−25)	7.119(−26)
	10^6	6.845(−24)	1.958(−24)	7.102(−25)	2.220(−25)	6.998(−26)
	10^7	8.777(−24)	2.004(−24)	6.872(−25)	2.151(−25)	6.874(−26)
	10^8	1.338(−23)	2.155(−24)	6.609(−25)	2.039(−25)	6.611(−26)
	10^9	2.635(−23)	2.533(−24)	6.308(−25)	1.827(−25)	5.903(−26)
$4 - 2$	10^2	1.220(−24)	5.302(−25)	2.331(−25)	8.246(−26)	2.758(−26)
	10^4	1.425(−24)	5.536(−25)	2.350(−25)	8.235(−26)	2.754(−26)
	10^6	2.052(−24)	6.103(−25)	2.381(−25)	8.162(−26)	2.732(−26)
	10^7	2.874(−24)	6.669(−25)	2.394(−25)	8.030(−26)	2.691(−26)
	10^8	4.846(−24)	7.723(−25)	2.399(−25)	7.659(−26)	2.549(−26)
	10^9	1.105(−23)	1.036(−24)	2.527(−25)	7.237(−26)	2.317(−26)
$5 - 2$	10^2	4.925(−25)	2.248(−25)	1.044(−25)	3.903(−26)	1.348(−26)
	10^4	5.928(−25)	2.387(−25)	1.061(−25)	3.910(−26)	1.347(−26)
	10^6	9.071(−25)	2.737(−25)	1.098(−25)	3.904(−26)	1.338(−26)
	10^7	1.344(−24)	3.102(−25)	1.124(−25)	3.846(−26)	1.308(−26)
	10^8	2.550(−24)	3.958(−25)	1.197(−25)	3.741(−26)	1.227(−26)
	10^9	6.688(−24)	6.100(−25)	1.423(−25)	3.852(−26)	1.189(−26)

Table 5d. He II line emissivities [erg cm^3 s^{-1}]: Case A

	N_e	T[K]			
$n_u - n_l$	[cm^{-3}]	1000	3000	10 000	30 000
$3 - 2$	10^4	5.079(−23)	2.064(−23)	7.197(−24)	2.496(−24)
	10^6	5.417(−23)	2.039(−23)	7.035(−24)	2.456(−24)
	10^7	5.969(−23)	2.044(−23)	6.904(−24)	2.420(−24)
	10^8	7.237(−23)	2.093(−23)	6.745(−24)	2.367(−24)
	10^9	1.030(−22)	2.253(−23)	6.589(−24)	2.293(−24)
$4 - 2$	10^4	1.104(−23)	5.181(−24)	2.152(−24)	8.590(−25)
	10^6	1.340(−23)	5.509(−24)	2.175(−24)	8.581(−25)
	10^7	1.611(−23)	5.844(−24)	2.196(−24)	8.565(−25)
	10^8	2.146(−23)	6.407(−24)	2.227(−24)	8.525(−25)
	10^9	3.341(−23)	7.403(−24)	2.269(−24)	8.417(−25)
$4 - 3$	10^4	1.205(−23)	4.535(−24)	1.397(−24)	4.192(−25)
	10^6	1.201(−23)	4.278(−24)	1.328(−24)	4.056(−25)
	10^7	1.254(−23)	4.118(−24)	1.270(−24)	3.935(−25)
	10^8	1.419(−23)	3.994(−24)	1.196(−24)	3.763(−25)
	10^9	1.862(−23)	4.013(−24)	1.112(−24)	3.528(−25)
$5 - 3$	10^4	3.572(−24)	1.549(−24)	5.634(−25)	1.925(−25)
	10^6	4.101(−24)	1.587(−24)	5.573(−25)	1.900(−25)
	10^7	4.678(−24)	1.620(−24)	5.499(−25)	1.872(−25)
	10^8	5.802(−24)	1.680(−24)	5.378(−25)	1.824(−25)
	10^9	8.323(−24)	1.808(−24)	5.197(−25)	1.738(−25)

Where comparison can be made, our emissivities for H I and H II, extrapolated to zero electron density, are in good agreement with those of Martin (1988). Differences are always less than two percent.

The highest temperature for which results are given for H I is 30 000 K. At this temperature, and with the hydrogen ionization fractions typical of gaseous nebulae, there will be significant collisional excitation from the ground state to the low-lying states of interest in this work. The values given in the tables for 30 000 K were calculated assuming that there is no such collisional excitation, and should therefore only be used if a) it is known that the fraction of neutral hydrogen is very low (see HS for the permitted range of values), or b) it is required to interpolate the tables to some intermediate temperature. Collisional excitation from the ground state is negligible at the next-lowest tabulated temperature (10 000 K).

5. Applications and discussion

5.1. Appearance of the H and He lines

Figures 1a–c show the components and their predicted intensities for the three selected lines Hα, Hβ and Hγ. In the figures, the vertical bars have a length proportional to the relative intensity of the component for the Case B, $T_e = 5000$ K and $N_e = 10^4$ cm^{-3}. The smooth curves represent a convolution of these intensities with the thermal velocity expected in a 5000 K plasma for H ($FWHM = 15.1$ km s^{-1}). They are however arbitrarily normalized, for presentation purposes. The H I Balmer lines each have seven components, with the total velocity range shrinking from 9.1 to 5.0 km s^{-1} between Hα and Hγ. For Hα, the convolved profile is double-peaked if the total broadening velocity is not more than 5 km s^{-1}; it is single but noticeably non-Gaussian for 7 km s^{-1}, and is difficult to distinguish from Gaussian for a total velocity over 11 km s^{-1}.

Figures 2a–d show the components and their predicted intensities for the four selected lines of He for the Case B, $T_e = 10\,000$ K and $N_e = 10^4$ cm^{-3}. A convolution of these intensities was calculated for a 10 000 K plasma ($FWHM = 10.7$ km s^{-1}).

At a given plasma temperature, the component spread is four times greater and the thermal velocity is two times smaller. He II 4686 Å is mainly broadened by the effect of two strong components situated 6.42 km s^{-1} apart. As can be seen from Fig. 2a, the weak components in the blue part of the line profile should not be interpreted as a blue-shifted emission line gas moving at -25 km s^{-1}! The effect on the $n = 5 \rightarrow 3$ line at 3203 Å is quite similar (Fig. 2b).

However, there are larger effects on the $3 \rightarrow 2$ and $4 \rightarrow 2$ lines in the ultraviolet (Figs. 2c,d). The 1640 Å and 1215 Å lines are clearly doubled when the only broadening is thermal, with peak-to-peak splittings of about 25 and 20 km s^{-1} respectively.
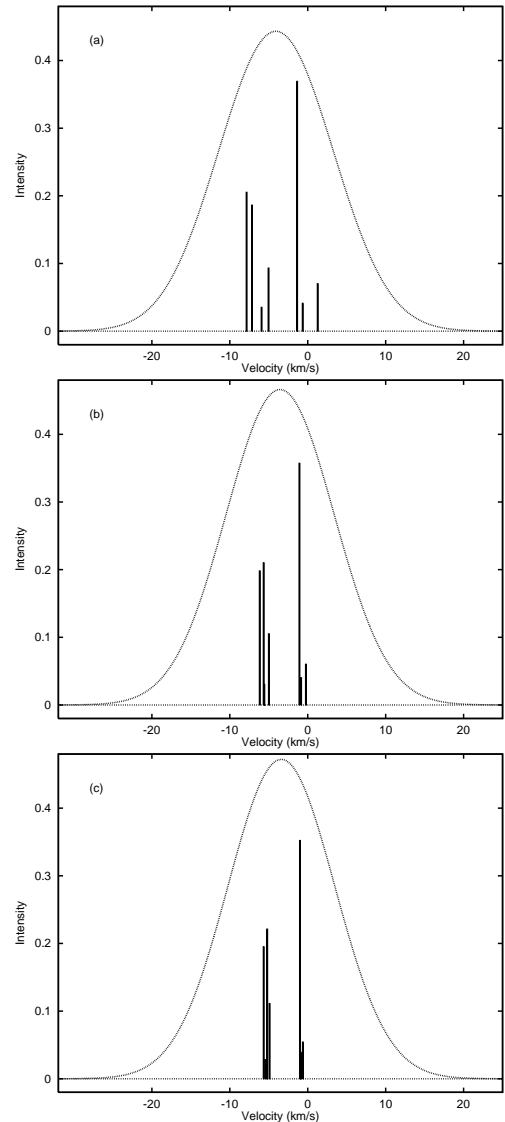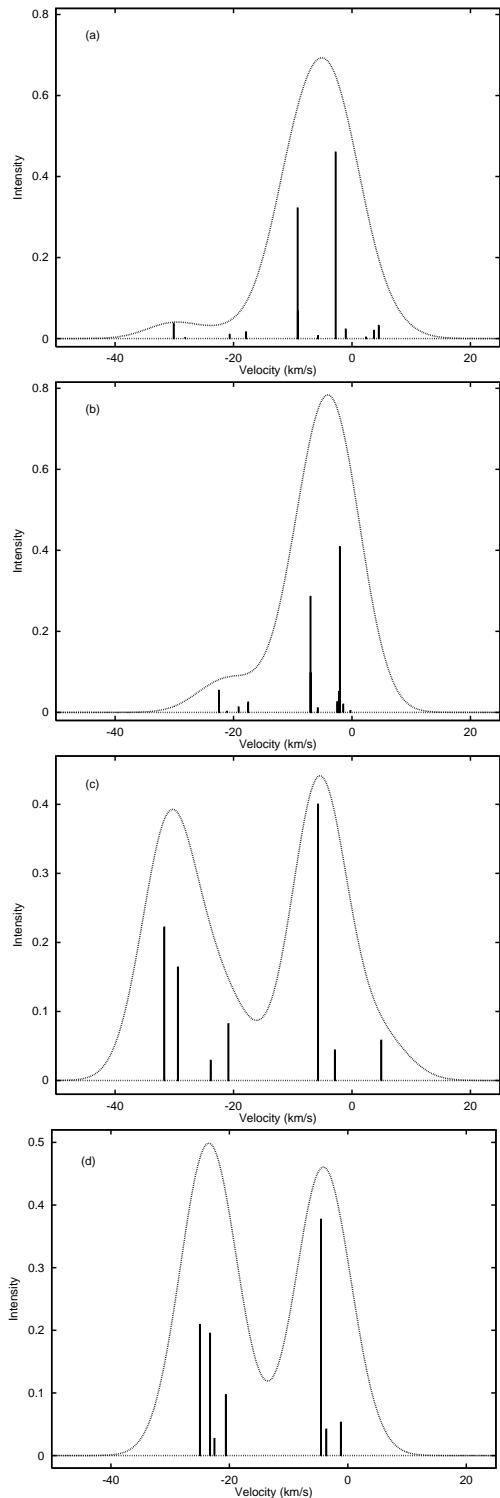

Fig. 1. Profiles of the H I emission lines in velocity space: **a)** – Hα, **b)** – Hβ, **c)** – Hγ. The vertical bars show the position and the relative intensity of the seven components of these lines for the Case B, $T_e = 5000$ K and $N_e = 10^4$ cm^{-3}. The smooth curve shows these intensities convolved with a velocity of 15.1 km s^{-1}, the $FWHM$ for thermal broadening of H at 5000 K

He II widths may be used to measure the velocity gradients within expanding planetary nebulae. The expansion velocity in the outer regions may be measured from [O I], [O II] or [N II] lines, in the central region from [O III] lines, and in the inner zones from He II lines such as 1640 or 4686 Å. Correction of the He II line widths for fine-structure will tend to steepen the derived gradient of expansion velocity with radius.

5.2. Line shifts

Accurate line centre positions are required both for precision radial velocity measurements and also for accurate

Fig. 2. Profiles of the He II emission lines in velocity space for the Case B, $T_e = 10\,000$ K and $N_e = 10^4\,\text{cm}^{-3}$: **a)** – He II 4686 Å line, **b)** – He II 3203 Å line, **c)** – He II 1215 Å line, **d)** – He II 1640 Å line. The smooth curve shows the component intensities convolved with a velocity of $10.7\,\text{km s}^{-1}$, the $FWHM$ for thermal broadening of He at $10\,000$ K

Table 6a. Line centre positions for H I (Case B). Entries show the decimal part of the mean wavelength, in Å

$n_u - n_l$	N_e [cm^{-3}]	300	1000	3000	10 000	30 000
$3 - 2$	10^2	.7969	.7954	.7930	.7910	.7900
	10^4	.7959	.7944	.7930	.7910	.7900
6562	10^6	.7935	.7930	.7920	.7905	.7900
	10^7	.7920	.7920	.7910	.7900	.7896
	10^8	.7881	.7891	.7886	.7881	.7881
	10^9	.7871	.7866	.7856	.7847	.7837
$4 - 2$	10^2	.3237	.3232	.3218	.3198	.3184
	10^4	.3237	.3228	.3218	.3198	.3184
4861	10^6	.3223	.3223	.3213	.3198	.3184
	10^7	.3213	.3213	.3208	.3193	.3179
	10^8	.3208	.3208	.3198	.3188	.3174
	10^9	.3237	.3232	.3228	.3213	.3188
$5 - 2$	10^2	.4619	.4609	.4604	.4590	.4575
	10^4	.4614	.4609	.4604	.4590	.4575
4340	10^6	.4609	.4604	.4600	.4590	.4575
	10^7	.4604	.4604	.4600	.4585	.4570
	10^8	.4624	.4619	.4609	.4595	.4580
	10^9	.4629	.4629	.4629	.4624	.4614

The header row of the table spans: $T[K]$ over columns 300, 1000, 3000, 10 000, 30 000.

calibration of Fabry-Perot high-resolution interferometers (Treffers 1981).

We have thus computed the "centres of gravity" of the emission lines we considered. These are calculated simply as the mean position of all the line components, each weighted by its relative intensity for the Case and physical conditions considered. This will correspond to the measured position of an emission line when it is completely unresolved. The mean wavelengths of the lines are given in Tables 6a–d; the tables show the decimal part of the mean wavelength in Å, with the integer part presented separately in the first column of the Table. Wavelengths are in air for $\lambda > 2000$ Å and in vacuum otherwise.

There are shifts in the line centres which are relevant for high-precision measurement of radial velocities or velocity fields. For a given Case (A or B) the maximum line centre shift with varying N_e or T_e is $0.6\,\text{km s}^{-1}$ for hydrogen (Hα, Case B) and $1.3\,\text{km s}^{-1}$ for helium ($\lambda1640$ Å, Case B). The largest shifts of one line between Case A and Case B are $0.9\,\text{km s}^{-1}$ for H (Hα) and $3.3\,\text{km s}^{-1}$ for He II ($\lambda1640$ Å).

Our computed shift between Cases A and B for Hα (0.9 km s^{-1}) is smaller than the value of 2.5 km s^{-1} reported by Dyson & Meaburn (1971). The relative intensities given in Table 3a do not differ significantly from the values given by Dyson & Meaburn (1971) (for $T_e = 10\,000$ K). Another possible source of the disagreement

Table 6b. Line centre positions for He II (Case B). Entries show the decimal part of the mean wavelength, in Å

$n_u - n_l$	N_e [cm^{-3}]	T[K] 1000	3000	10 000	30 000
3 − 2	10^4	.4196	.4182	.4160	.4138
	10^6	.4185	.4176	.4156	.4136
1640	10^7	.4175	.4167	.4152	.4133
	10^8	.4161	.4159	.4144	.4130
	10^9	.4144	.4143	.4137	.4125
4 − 2	10^4	.1337	.1329	.1317	.1300
	10^6	.1333	.1327	.1315	.1299
1215	10^7	.1329	.1323	.1313	.1299
	10^8	.1322	.1320	.1310	.1298
	10^9	.1311	.1310	.1302	.1293
4 − 3	10^4	.7534	.7515	.7480	.7446
	10^6	.7515	.7500	.7471	.7441
4685	10^7	.7500	.7480	.7466	.7441
	10^8	.7476	.7471	.7456	.7437
	10^9	.7456	.7451	.7437	.7427
5 − 3	10^4	.1301	.1282	.1252	.1213
	10^6	.1287	.1274	.1250	.1211
3203	10^7	.1274	.1267	.1243	.1206
	10^8	.1260	.1255	.1230	.1201
	10^9	.1233	.1228	.1221	.1191

Table 6d. Line centre positions for He II (Case A). Entries show the decimal part of the mean wavelength, in Å

$n_u - n_l$	N_e [cm^{-3}]	T[K] 1000	3000	10 000	30 000
3 − 2	10^4	.4285	.4285	.4290	.4302
	10^6	.4283	.4286	.4291	.4301
1640	10^7	.4287	.4287	.4291	.4303
	10^8	.4287	.4288	.4293	.4304
	10^9	.4290	.4291	.4296	.4307
4 − 2	10^4	.1422	.1422	.1418	.1415
	10^6	.1422	.1421	.1418	.1416
1215	10^7	.1422	.1421	.1418	.1416
	10^8	.1420	.1420	.1417	.1416
	10^9	.1416	.1416	.1416	.1415
4 − 3	10^4	.7529	.7500	.7456	.7412
	10^6	.7505	.7485	.7446	.7397
4685	10^7	.7480	.7466	.7432	.7393
	10^8	.7456	.7446	.7422	.7388
	10^9	.7427	.7422	.7402	.7373
5 − 3	10^4	.1313	.1296	.1270	.1230
	10^6	.1301	.1289	.1265	.1228
3203	10^7	.1292	.1279	.1260	.1226
	10^8	.1277	.1270	.1248	.1218
	10^9	.1252	.1250	.1233	.1208

Table 6c. Line centre positions for H I (Case A). Entries show the decimal part of the mean wavelength, in Å

$n_u - n_l$	N_e [cm^{-3}]	T[K] 300	1000	3000	10 000	30 000
3 − 2	10^2	.8052	.8057	.8062	.8076	.8105
	10^4	.8052	.8057	.8062	.8076	.8110
6562	10^6	.8057	.8062	.8066	.8081	.8110
	10^7	.8062	.8062	.8066	.8081	.8110
	10^8	.8052	.8057	.8062	.8076	.8105
	10^9	.8018	.8018	.8027	.8042	.8062
4 − 2	10^2	.3325	.3320	.3320	.3315	.3315
	10^4	.3320	.3320	.3320	.3315	.3315
4861	10^6	.3320	.3320	.3320	.3315	.3315
	10^7	.3315	.3320	.3315	.3315	.3315
	10^8	.3301	.3306	.3306	.3306	.3306
	10^9	.3276	.3281	.3286	.3281	.3276
5 − 2	10^2	.4692	.4692	.4692	.4688	.4683
	10^4	.4692	.4692	.4692	.4688	.4683
4340	10^6	.4692	.4692	.4688	.4688	.4683
	10^7	.4683	.4688	.4688	.4683	.4678
	10^8	.4668	.4673	.4673	.4668	.4663
	10^9	.4644	.4648	.4648	.4648	.4644

could be the data used for the energy levels. We use the results from Erickson (1977) with the Lamb shift included while Dyson & Meaburn (1971) use relativistic theory but excluding the Lamb shift. The differences in level energies are not, however, sufficient to explain the discrepancy, indicating that the value of 2.5 km s^{-1} given by Dyson & Meaburn (1971) is in error.

5.3. The Hα–[N II] method for deriving electron temperature

Because the thermal $FWHM$ of an emission line varies with temperature and ionic mass as $T_e^{1/2}\,m^{-1/2}$, the electron temperature T_e can in principle be derived from the different observed widths of different ionic lines (Wilson et al. 1959). Observationally the easiest line pair to work with (Courtes et al. 1968) is Hα and [N II]6584 Å, which are only separated by 21 Å. The basic assumption is that the emissivity of the two lines samples the velocity field (mainly, expansion and turbulence) in identical ways. While this may be true for some H II regions, it is frequently untrue for planetary nebulae, where N$^+$ ions are often only located at the outer edge.

Meaburn (1970) showed that the fine structure of Hα would affect the resulting derived electron temperature, and Dyson & Meaburn (1971) gave correction factors to be

Table 7. $FWHM$ and broadening term δ [km s^{-1}] for Hα

v_{broad}	$FWHM$	δ
3.0	9.41	8.914
3.5	9.89	9.245
4.0	10.32	9.514
4.5	10.73	9.739
5.0	11.10	9.910
6.0	11.70	10.049
7.0	12.09	9.860
8.0	12.41	9.487
9.0	12.82	9.135
10.0	13.35	8.850
12.0	14.68	8.454
14.0	16.23	8.209
16.0	17.91	8.048
18.0	19.67	7.939
20.0	21.49	7.863
22.0	23.34	7.804
24.0	25.22	7.762
26.0	27.12	7.727
30.0	30.97	7.678
35.0	35.82	7.639
40.0	40.72	7.618
50.0	50.57	7.591
100.0	100.28	7.549

used for the Hα widths. Since our results are significantly different, we give in Table 7 new correction factors.

We make the above assumption and further assume that there are expansion and turbulent fields which contribute in quadrature to the total $FWHM$ of observed line profiles. Then the $FWHM$ of Hα and [N II] are, in velocity units,

$$F(\text{H}\alpha)^2 = 8\ln2\,(kT_e/m_H)\,+\delta^2+v_e^2+v_t^2\,, \qquad (7)$$

$$F(\text{N II})^2 = 8\ln2\,(kT_e/m_N)\,+v_e^2+v_t^2\,, \qquad (8)$$

where δ is defined as that width which adds in quadrature to broaden the Hα line to allow for the fine-structure, v_e and v_t are the $FWHM$ of expansion and turbulent velocity fields, and m_H and m_N are the masses of the hydrogen and nitrogen atoms respectively. From Eqs. (7)–(8), the solution for the electron temperature is

$$T_e = \frac{\left(F(\text{H}\alpha)^2 - \delta^2 - F(\text{N II})^2\right)}{(8k\,\ln2\,[1/m_H - 1/m_N])}\,. \qquad (9)$$

The reason that a single value of δ cannot be given in Table 7 is that the presence of seven unequal components within the line produces a complex effect on the final $FWHM$. We have computed δ by convolving our computed Hα component intensities with a Gaussian profile corresponding to a *total* velocity v_{broad} which represents the combined effect of all broadening processes other than the fine-structure (thermal, instrumental, expansion and turbulent). We determine the $FWHM$ of the resultant profile empirically by searching the profile for the points at half peak intensity. The quantity δ is then obtained by subtracting v_{broad} from the $FWHM$ of the profile in quadrature and is thus the *effective* additional velocity width of the profile due to the fine-structure.

The results are given in Table 7. It can be seen that δ is a very slowly-varying function of the total broadening velocity, and so interpolation in the table should be quite accurate.

References

Baker J.G., Menzel D.H., 1938, ApJ 88, 52
Brink D.M., Satchler G.R., 1968, "Angular Momentum". Oxford University Press
Courtes G., Louise R., Monnet G., 1968, Ann. d'Ap. 31, 493
Cumming R.J., Meikle W.P.S., 1993, MNRAS 262, 689
Dyson J.E., Meaburn J., 1971, A&A 12, 219
Erickson G.W., 1977, J. Phys. Chem. Ref. Data 6, 831
Ferguson A.I., 1986, Phys. Bull. 37, 330
Gallagher J.S., Hunter D.A., 1983, ApJ 274, 141
Hänsch T.W., Lee S.A., Wallenstein R., Wieman C., 1975, Phys. Rev. Lett. 34, 307
Hummer D.G., Storey P.J., 1987, MNRAS 224, 801
Laming J.M., Feldman U., 1993, ApJ 403, 434
Martin P.G., 1988, ApJS 66, 125
Meaburn J., 1970, Nat 228, 44
Onello J.S., Phillips J.A., 1993, Proc. 104th ASP Meeting, Casssinelli J.P. & Churchwell E.B. (eds.) ASP Conf. Ser. 35, 366
Smits D.P., 1991, MNRAS 248, 193
Storey P.J., Hummer D.G., 1988, MNRAS 231, 1139
Storey P.J., Hummer D.G., 1991, Comp. Phys. Commun. 66, 129
Storey P.J., Hummer D.G., 1995, MNRAS 272, 41
Treffers R.R., 1981, PASP 93, 247
Williams R.E., Woolf N.J., Hege E.K., Moore R.L., Kopriva D.A., 1978, ApJ 224, 171
Wilson O.C., Munch G., Flather E.M., Coffeen M.F., 1959, ApJS 4, 199